

# Spectrum Analysis of Bright *Kepler* $\gamma$ Doradus Candidate Stars<sup>\*</sup>

A. Tkachenko,<sup>1</sup> H. Lehmann,<sup>2</sup> B. Smalley,<sup>3</sup> J. Debosscher,<sup>1</sup> and C. Aerts<sup>1,4</sup>

<sup>1</sup>*Instituut voor Sterrenkunde, K.U. Leuven, Celestijnenlaan 200D, B-3001 Leuven, Belgium*

<sup>2</sup>*Thüringer Landessternwarte Tautenburg, 07778 Tautenburg, Germany*

<sup>3</sup>*Astrophysics Group, Keele University, Staffordshire ST5 5BG, United Kingdom*

<sup>4</sup>*Department of Astrophysics, IMAPP, Radboud University Nijmegen, 6500 GL Nijmegen, The Netherlands*

Received date; accepted date

## ABSTRACT

Ground-based spectroscopic follow-up observations of the pulsating stars observed by the *Kepler* satellite mission are needed for their asteroseismic modelling. We aim to derive the fundamental parameters for a sample of 26  $\gamma$  Doradus candidate stars observed by the *Kepler* satellite mission to accomplish one of the required preconditions for their asteroseismic modelling and to compare our results with the types of pulsators expected from the existing light curve analysis. We use the spectrum synthesis method to derive the fundamental parameters like  $T_{\text{eff}}$ ,  $\log g$ ,  $[M/H]$ , and  $v \sin i$  from newly obtained spectra and compute the spectral energy distribution from literature photometry to get an independent measure of  $T_{\text{eff}}$ . We find that most of the derived  $T_{\text{eff}}$  values agree with the values given in the Kepler Input Catalogue. According to their positions in the HR-diagram three stars are expected  $\gamma$  Dor stars, ten stars are expected  $\delta$  Sct stars, and seven stars are possibly  $\delta$  Sct stars at the hot border of the instability strip. Four stars in our sample are found to be spectroscopic binary candidates and four stars have very low metallicity where two show about solar C abundance. Six of the 10 stars located in the  $\delta$  Sct instability region of the HR-diagram show both  $\delta$  Sct and  $\gamma$  Dor-type oscillations in their light curves implying that  $\gamma$  Dor-like oscillations are much more common among the  $\delta$  Sct stars than predicted by theory. Moreover, seven stars showing periods in the  $\delta$  Sct and the  $\delta$  Sct- $\gamma$  Dor range in their light curves are located in the HR-diagram left of the blue edge of the theoretical  $\delta$  Sct instability strip. The consistency of these findings with recent investigations based on high-quality *Kepler* data implies the need for a revision of the theoretical  $\gamma$  Dor and  $\delta$  Sct instability strips.

**Key words:** Stars: variables: delta Scuti – Stars: fundamental parameters – Stars: abundances.

## 1 INTRODUCTION

The *Kepler* satellite was launched in March 2009 with the primary goal to search for transiting exoplanets in the solar neighbourhood. It delivers single band-pass light curves of micromagnitude precision and has found hundreds of planet candidates (Borucki et al. 2011). The long, uninterrupted, and high-precision time series photometry taken for a huge number of stars has also led to the discovery of many new pulsating stars and is an ideal basis for an in-depth asteroseismic analysis (see e.g. Gilliland et al. 2010). For this analysis and the subsequent asteroseismic modelling, pre-

cise knowledge of the fundamental parameters of the stars is essential. These parameters cannot be determined from the single band-pass photometry delivered by *Kepler* alone, however. Hence, ground-based spectroscopic follow-up observations have been undertaken to determine the stellar parameters.

In this paper, we are concerned with  $\gamma$  Doradus candidates found from data assembled with the *Kepler* mission. Such pulsators are named after their prototype, Gamma Doradus, whose multiperiodic variable nature was first reported by Cousins (1992). Krisciunas et al. (1993) discovered a multiperiodic photometric variability with an amplitude of about 0.1 mag and periods of 2.275 and 1.277 d in 9 Aurigae and reported on similar behaviour in  $\gamma$  Doradus and HD 96008. Following these discoveries, Balona et al. (1994)

<sup>\*</sup> Based on observations with the 2-m Alfred-Jensch-Telescope of the Thüringer Landessternwarte Tautenburg

**Table 1.** Journal of observations. N gives the number of obtained spectra, V - the visual magnitude. All spectra have been taken in 2010.

KIC	Designation	N	V	SpT	Observed
01 571 152	BD+36 3535	2	9.3	F0	May-June
02 166 218	BD+37 3490	3	9.5	F0	May-June
03 217 554	BD+38 3415	2	9.6	A5	September
03 453 494	BD+38 3666	3	9.6	A5	September
04 847 411	HD 225314	4	9.8	A7	June-July
05 088 308	HD 180099	1	8.7	F5	May
05 164 767	HD 175537	6	7.8	F0	April-June
05 446 068	BD+40 3704	7	9.7	—	June-July
05 785 707	HD 181902	3	9.0	A	August
06 289 468	BD+41 3389	5	9.4	A2	May
06 509 175	BD+41 3248	2	10.0	A2	August
06 587 551	BD+41 3207	3	9.8	A0	June-July
06 756 386	HD 175939	2	8.7	A2	August
07 748 238	HD 181985	2	9.5	A	May-July
08 623 953	BD+44 3134	3	9.3	A5	August
08 738 244	HD 176390	2	8.1	A3	August
08 750 029	BD+44 3113	3	9.7	A5	June
09 413 057	BD+45 2954	5	9.6	A2	May-June
09 764 965	HD 181206	2	8.8	A5	August
09 812 351	HD 174019	3	7.9	A0	April-May
10 119 517	TYC 3544-1245-1	3	9.9	—	August
10 451 090	HD 174789	3	9.2	A	August
10 616 594	TYC 3561-971-1	3	9.8	—	August
10 977 859	HD 184333	2	8.8	A2	August
11 498 538	HD 178874	2	7.3	F5	September
12 353 648	HD 234859	3	9.6	A2	August

introduced a new class of variable stars named after the prototype star  $\gamma$  Doradus.  $\gamma$  Dor stars are assumed to pulsate in high-order, low-degree non-radial gravity modes driven by the flux blocking mechanism near the base of their convective zones (Guzik et al. 2000; Dupret et al. 2005). The typical masses of these stars lie in the range of 1.5–1.8  $M_{\odot}$  (Aerts et al. 2010). According to Kaye et al. (1999),  $\gamma$  Dor-type stars can be characterised as follows: (1) spectral type A7–F5 and luminosity class IV, IV-V, or V, (2) low-amplitude photometric variations with periods between 0.5 and 3 days as well as spectroscopic variability seen as both line-profile and low-amplitude radial velocity (RV) variations.

$\gamma$  Dor stars are located close to the red edge of the classical instability strip in the HR-diagram. The theoretical  $\gamma$  Dor instability strip overlaps with the red edge of classical instability strip where the  $\delta$  Sct pulsators are located. While the low-order p-modes of  $\delta$  Sct stars are characterized by short periods ranging from 18 min to 8 h, typical  $\gamma$  Dor high-order g-modes have periods of the order of a day (e.g., Aerts et al. 2010). Multiperiodicity is found for most of the  $\gamma$  Dor class members from ground-based photometry (Henry et al. 2007; Cuypers et al. 2009) and spectroscopy (e.g., Mathias et al. 2004; De Cat et al. 2006). Pulsators in the overlapping region of the  $\delta$  Sct and  $\gamma$  Dor instability strip are expected to show the two pulsation characteristics, i.e., high-order g-modes probing the core and low-order p- and g-modes probing the outer layers. While the frequency patterns of these two types of oscillations are in principle easy to distinguish in the co-rotating frame of reference, the fre-

quencies start to overlap in an inertial frame of reference, particularly for the fast rotators. Moreover, the overall beating patterns are complex and hard to unravel from interrupted ground-based data. Some hybrid pulsators were already found previously (e.g., Rowe et al. 2006; King et al. 2007), but the *Kepler* data make it clear that hybrid pulsators turn out to be numerous, both for AF-type stars (Uytterhoeven et al. 2011b; Balona et al. 2011a) and for B-type stars (Balona et al. 2011b).

Gray & Kaye (1999) were the first to report a connection between the  $\lambda$  Bootis ( $\lambda$  Boo) type stars and the  $\gamma$  Dor variables.  $\lambda$  Boo stars are Pop I hydrogen burning metal poor (except of C, N, O, and S) A-type stars (Paunzen et al. 1997; Paunzen 2004) showing significant underabundances of Fe-peak elements (up to  $-2$  dex compared to the solar composition). They belong to the class of non-magnetic, chemically peculiar stars. Up to now, only two further reports (Sadakane 2006; Rodríguez et al. 2007) on a possible connection between the  $\lambda$  Boo stars and  $\gamma$  Dor-type variability appeared. A recent analysis of a sample of 18  $\gamma$  Dor stars performed by Bruntt et al. (2008) revealed no principal difference between the abundances of the analysed stars and the chemical composition of non-pulsating A- and F-type stars.

In this paper, we investigate a sample of 26 among the brighter stars in the *Kepler* field which have been proposed to be candidates for  $\gamma$  Dor variables (Uytterhoeven et al. 2011a). We aim to evaluate fundamental stellar parameters like effective temperature  $T_{\text{eff}}$ , surface gravity  $\log g$ , projected rotational velocity  $v \sin i$ , and microturbulent velocity  $\xi$  as well as the chemical composition of the target stars from newly obtained high-resolution spectra. Based on the derived parameters, we present a classification of the sample stars according to the expected type of variability. The derived chemical composition in turn allows to check for a possible connection between  $\gamma$  Dor-type variability and  $\lambda$  Boo-type abundance patterns.

## 2 OBSERVATIONS

We base our analysis on high-resolution, high signal-to-noise ratio (S/N) spectra taken with the Coudé-Echelle spectrograph attached to the 2-m telescope of the Thüringer Landessternwarte Tautenburg, Germany. The spectra have a resolution of 32000 and cover the wavelength range from 4720 to 7400 Å. Table 1 represents the journal of observations and gives the Kepler Input Catalog (KIC) number, an alternative designation, the number of obtained spectra, the visual magnitude, the spectral type as is indicated in the SIMBAD database, and the period of observations in 2010. The number of acquired spectra is different for different stars since we aimed to reach a S/N of about 100 for the mean, averaged spectrum of each object.

The data have been reduced using standard ESO-MIDAS packages. The data reduction included bias and stray-light subtraction, cosmic rays filtering, flat fielding by a halogen lamp, wavelength calibration by a ThAr lamp, and normalisation to the local continuum. All spectra were additionally corrected in wavelength for individual instrumental shifts by using a large number of telluric O<sub>2</sub> lines. The cross-correlation technique was used to estimate the RVs from the

**Table 2.** Fundamental stellar parameters. The values labeled with “K” are taken from the KIC and given for comparison. Metallicity values labeled with “(Fe)” refer to the derived Fe-abundance.

KIC	$T_{\text{eff}}^{\text{K}}(K)$	$\log g^{\text{K}}$	$[M/H]^{\text{K}}$	$T_{\text{eff}}(K)$	$\log g$	$[M/H]$	$v \sin i$ (km s $^{-1}$ )	$\xi$ (km s $^{-1}$ )	SpT <sup>K</sup>	SpT
01 571 152 <sup>1)</sup>	7048	3.164	+0.05	7065 $^{+79}_{-79}$	4.46 $^{+0.23}_{-0.38}$	-0.18 $^{+0.10}_{-0.10}$	90.1 $^{+8.3}_{-12.7}$	2.03 $^{+0.46}_{-0.49}$	F0.5 III	F1 V
02 166 218	7153	3.345	-0.11	7062 $^{+56}_{-56}$	3.88 $^{+0.17}_{-0.21}$	-0.37 $^{+0.07}_{-0.07}$	99.7 $^{+3.5}_{-3.5}$	2.82 $^{+0.23}_{-0.26}$	F0 IV-III	F1 IV
03 217 554 <sup>1)</sup>	7801	3.504	+0.06	7667 $^{+66}_{-66}$	2.78 $^{+0.10}_{-0.09}$	-1.20(Fe)	225.5 $^{+17.0}_{-17.2}$	4.82 $^{+0.75}_{-0.74}$	A6.5 IV-III	A7.5 III-II
03 453 494	7806	3.843	-0.33	7737 $^{+57}_{-57}$	3.71 $^{+0.21}_{-0.22}$	-0.95(Fe)	210.8 $^{+14.5}_{-14.5}$	3.24 $^{+0.66}_{-0.60}$	A7 IV	A7 IV
04 847 411 <sup>RV)</sup>	6563	4.517	-1.95	7466 $^{+50}_{-50}$	3.83 $^{+0.24}_{-0.24}$	-0.52 $^{+0.09}_{-0.09}$	139.9 $^{+6.4}_{-6.2}$	2.62 $^{+0.33}_{-0.33}$	F4 V	A8.5 V-IV
05 088 308 <sup>1)</sup>	6567	4.035	-0.68	6708 $^{+37}_{-37}$	2.67 $^{+0.13}_{-0.14}$	-0.35 $^{+0.06}_{-0.07}$	40.7 $^{+1.2}_{-1.2}$	4.01 $^{+0.17}_{-0.17}$	F4 V-IV	F4 III-II
05 164 767 <sup>RV)</sup>	—	—	—	6933 $^{+76}_{-76}$	3.59 $^{+0.39}_{-0.32}$	-0.19 $^{+0.11}_{-0.12}$	163.9 $^{+8.7}_{-8.6}$	2.62 $^{+0.47}_{-0.41}$	—	F1.5 IV
05 446 068 <sup>1,2)</sup>	5337	4.476	-0.69	5763 $^{+90}_{-90}$	3.37 $^{+0.25}_{-0.26}$	+0.24 $^{+0.10}_{-0.10}$	7.8 $^{+2.1}_{-2.2}$	0.0 <sup>fixed</sup>	G9.5 V	F9.5 IV
05 785 707	8009	3.615	-0.14	7965 $^{+70}_{-70}$	3.37 $^{+0.15}_{-0.09}$	-0.56 $^{+0.11}_{-0.11}$	171.3 $^{+10.4}_{-10.0}$	2.84 $^{+0.45}_{-0.48}$	A5.5 IV	A6 IV-III
06 289 468 <sup>RV)</sup>	8267	3.741	-0.30	8107 $^{+70}_{-70}$	3.30 $^{+0.06}_{-0.06}$	-0.48 $^{+0.11}_{-0.10}$	149.7 $^{+7.0}_{-7.4}$	2.67 $^{+0.41}_{-0.39}$	A4.5 IV	A5 III
06 509 175	7299	3.522	-0.21	7510 $^{+50}_{-50}$	3.20 $^{+0.25}_{-0.26}$	-0.45 $^{+0.10}_{-0.10}$	132.4 $^{+7.8}_{-7.2}$	2.81 $^{+0.43}_{-0.39}$	A9 IV-III	A8 III
06 587 551	8377	3.929	-0.07	8826 $^{+144}_{-144}$	3.76 $^{+0.07}_{-0.07}$	-0.11 $^{+0.12}_{-0.12}$	139.8 $^{+7.9}_{-8.1}$	2.80 $^{+0.53}_{-0.90}$	A4 V-IV	A2.5 IV
06 756 386	7992	3.513	-0.51	7891 $^{+62}_{-62}$	3.19 $^{+0.09}_{-0.08}$	-0.59 $^{+0.10}_{-0.10}$	192.8 $^{+11.6}_{-11.8}$	2.99 $^{+0.52}_{-0.49}$	A6 IV-III	A6 III
07 748 238	7228	3.470	-0.22	7264 $^{+58}_{-58}$	3.96 $^{+0.20}_{-0.25}$	-0.37 $^{+0.08}_{-0.08}$	120.8 $^{+4.8}_{-4.9}$	3.53 $^{+0.33}_{-0.38}$	A9.5 IV-III	A9.5 V-IV
08 623 953	7725	3.738	-0.11	7726 $^{+50}_{-50}$	3.43 $^{+0.18}_{-0.17}$	-0.35 $^{+0.08}_{-0.08}$	84.8 $^{+3.2}_{-3.3}$	2.76 $^{+0.29}_{-0.29}$	A7 IV	A7 IV-III
08 738 244	8167	4.152	+0.41	8154 $^{+96}_{-96}$	3.24 $^{+0.07}_{-0.08}$	-0.27 $^{+0.12}_{-0.12}$	133.9 $^{+7.1}_{-7.1}$	2.70 $^{+0.42}_{-0.67}$	A5 V-IV	A5 III
08 750 029	—	—	—	7341 $^{+59}_{-59}$	3.70 $^{+0.27}_{-0.23}$	-0.56 $^{+0.10}_{-0.10}$	166.1 $^{+8.8}_{-8.4}$	2.95 $^{+0.46}_{-0.41}$	—	A9 IV
09 413 057 <sup>RV)</sup>	8465	3.868	-0.06	8588 $^{+97}_{-97}$	3.59 $^{+0.05}_{-0.05}$	-0.56 $^{+0.15}_{-0.12}$	171.0 $^{+10.6}_{-10.4}$	2.83 $^{+0.57}_{-0.60}$	A4 V-IV	A3 IV
09 764 965	7455	4.085	-0.18	7478 $^{+41}_{-41}$	3.74 $^{+0.17}_{-0.18}$	-0.27 $^{+0.06}_{-0.06}$	85.1 $^{+2.5}_{-2.5}$	3.55 $^{+0.24}_{-0.24}$	A8.5 V-IV	A8 IV
09 812 351	7794	3.470	-0.29	7833 $^{+62}_{-62}$	3.20 $^{+0.15}_{-0.11}$	-0.90(Fe)	55.6 $^{+3.5}_{-3.2}$	2.18 $^{+0.40}_{-0.32}$	A6.5 IV-III	A6 III
10 119 517 <sup>RV)</sup>	6225	4.375	-0.45	6438 $^{+69}_{-69}$	4.21 $^{+0.22}_{-0.13}$	-0.24 $^{+0.07}_{-0.07}$	77.9 $^{+3.4}_{-3.3}$	1.26 $^{+0.30}_{-0.27}$	F8 V	F5 V
10 451 090	7577	4.134	-0.05	7633 $^{+50}_{-50}$	3.58 $^{+0.15}_{-0.15}$	+0.04 $^{+0.06}_{-0.06}$	44.2 $^{+1.5}_{-1.5}$	3.00 $^{+0.16}_{-0.16}$	A8 V-IV	A7.5 IV-III
10 616 594 <sup>2)</sup>	5161	3.762	-0.75	5327 $^{+88}_{-88}$	2.81 $^{+0.25}_{-0.22}$	+0.16 $^{+0.13}_{-0.20}$	7.24 $^{+0.9}_{-0.8}$	0.63 $^{+0.20}_{-0.25}$	G8.5 V-IV	G3.5 III
10 977 859	8052	3.935	+0.15	8195 $^{+57}_{-57}$	3.60 $^{+0.07}_{-0.06}$	-0.11 $^{+0.07}_{-0.06}$	63.0 $^{+3.0}_{-2.9}$	3.08 $^{+0.28}_{-0.27}$	A5.5 V-IV	A5 IV
11 498 538 <sup>2)</sup>	6287	4.036	-0.29	6428 $^{+57}_{-57}$	2.90 $^{+0.14}_{-0.15}$	-0.15 $^{+0.07}_{-0.07}$	39.7 $^{+1.2}_{-1.1}$	2.54 $^{+0.19}_{-0.16}$	F7 V-IV	F5.5 III
12 353 648	7414	3.473	-0.38	7163 $^{+51}_{-51}$	3.49 $^{+0.23}_{-0.29}$	-1.05(Fe)	192.0 $^{+10.6}_{-10.6}$	2.32 $^{+0.42}_{-0.43}$	A8.5 IV-III	F0 IV-III

<sup>1)</sup> suspected SB2 star; <sup>2)</sup> no reliable fit obtained; <sup>RV)</sup> differences in the measured RVs are observed

individual spectra so that the single spectra finally could be shifted and added to build the mean, high S/N ratio averaged spectrum of each star. The RVs computed at this step have also been used to check for possible variations due to binarity, high-amplitude stellar oscillations and rotational modulation.

### 3 SPECTRAL ANALYSIS

#### 3.1 Method

The “classical” method of spectrum analysis by means of equivalent width measurements and subsequent fitting of the ionization equilibria of different elements requires the star to rotate slowly, so that a sufficient number of clean, unblended spectral lines can be identified and measured in the stellar spectrum. In the case of rapidly rotating stars, this

method fails due to the high percentage of blended lines. The method of spectrum synthesis, on the other hand, is based on the comparison between observed and theoretical spectra in a certain wavelength range. Its advantage is that the effect of line blending can be taken into account when computing the synthetic spectra and thus no restrictions with respect to the rotational velocity occur. Because of the large number of fast rotators in our sample, we use the second method comparing the observed spectra with a huge number of synthetic spectra computed on a grid in the stellar parameters. Against the much faster approach of solving the so-called inverse problem, i.e. to determine the physical parameter values directly from the observations using some non-linear optimization method, the grid search has the advantage that it will always determine the globally best solution if the grid is dense enough. Its principal disadvantage of much longer computing time plays no crucial role in our analysis since

**Table 3.** Derived metallicity and elemental abundances relative to solar ones in dex. Asterisks indicate elements with error estimates of  $\pm 0.10$  dex ( $\pm 0.20$  dex in all other cases). Metallicity values labeled with “(Fe)” refer to the derived Fe-abundance.

KIC	[M/H]	C	O	Mg	Si	Ca	Fe	Na	Sc	Ti	Cr	Mn	Y	Ba	V	Co	Ni	Zr
		-3.65	-3.38	-4.51	-4.53	-5.73	-4.59	-5.87	-8.99	-7.14	-6.40	-6.65	-9.83	-9.87	-8.04	-7.12	-5.81	-9.45
01 571 152	-0.18 <sup>+0.10</sup> <sub>-0.10</sub>	+0.05	—	-0.10*	-0.10	-0.25*	-0.15*	+0.00	+0.00	-0.25*	-0.15*	-0.15	-0.20	+0.80	—	—	-0.20*	—
02 166 218	-0.37 <sup>+0.07</sup> <sub>-0.07</sub>	-0.10	—	-0.15*	-0.20	-0.20*	-0.45*	-0.10	-0.35	-0.40*	-0.40*	-0.40	-0.35	+0.60	—	—	-0.45*	—
03 217 554	-1.20(Fe)	-1.10	—	-0.35*	-0.10	-1.35	-1.20*	—	-1.15	-1.05	-1.70	—	—	-1.10	—	—	-0.80	—
03 453 494	-0.95(Fe)	-0.60	—	-0.10*	-0.10	-1.25	-0.95*	—	-0.75	-0.95	-1.00	—	—	-1.05	—	—	-0.70	—
04 847 411	-0.52 <sup>+0.09</sup> <sub>-0.09</sub>	-0.20	—	-0.20*	-0.10	-0.70*	-0.55*	+0.05	-0.45	-0.75*	-0.55*	-0.40	—	+0.25	—	—	-0.50*	—
05 088 308	-0.35 <sup>+0.06</sup> <sub>-0.07</sub>	-0.30	—	-0.30*	-0.50	-0.25*	-0.50*	-0.30	-0.35	-0.55*	-0.45*	-0.45	-0.10	+0.40	—	—	-0.30*	—
05 164 767	-0.19 <sup>+0.11</sup> <sub>-0.12</sub>	+0.15	—	+0.00*	+0.15	-0.20*	-0.35*	+0.50	-0.05	-0.65*	-0.10*	-0.05	-0.60	+0.60	—	—	-0.25*	—
05 446 068	+0.24 <sup>+0.10</sup> <sub>-0.10</sub>	-0.30	—	+0.10*	-0.25*	-0.05*	+0.15*	+0.10	+0.20*	+0.30*	+0.25*	+0.35*	+0.25*	+0.50	+0.55*	+0.35*	+0.10*	+0.10
05 785 707	-0.56 <sup>+0.11</sup> <sub>-0.11</sub>	-0.20	—	-0.25*	+0.15	-0.50	-0.50*	—	-0.50	-0.85	-0.70	—	—	-0.40	—	—	-0.45	—
06 289 468	-0.48 <sup>+0.11</sup> <sub>-0.10</sub>	-0.30	—	+0.05*	-0.05	-0.75	-0.50*	—	-0.55	-0.65	-0.60	—	—	-0.50	—	—	-0.55	—
06 509 175	-0.45 <sup>+0.10</sup> <sub>-0.10</sub>	-0.15	—	-0.05*	+0.05	-0.35*	-0.55*	+0.10	-0.45	-0.65*	-0.55*	-0.20	—	-0.60	—	—	-0.45*	—
06 587 551	-0.11 <sup>+0.12</sup> <sub>-0.12</sub>	+0.00	+0.00	+0.20*	+0.30	-0.20	-0.10*	—	-0.05	-0.35	-0.10	—	—	-0.40	—	—	-0.15	—
06 756 386	-0.59 <sup>+0.12</sup> <sub>-0.12</sub>	-0.20	—	+0.00*	+0.20	-0.50	-0.65*	—	-0.75	-0.70	-0.65	—	—	-1.30	—	—	-0.60	—
07 748 238	-0.37 <sup>+0.10</sup> <sub>-0.10</sub>	-0.15	—	-0.10*	+0.00	-0.25*	-0.45*	+0.10	-0.35	-0.45*	-0.45*	-0.35	—	+0.50	—	—	-0.40*	—
08 623 953	-0.35 <sup>+0.10</sup> <sub>-0.10</sub>	-0.10	—	-0.10*	+0.00	-0.25	-0.40*	+0.10	-0.35	-0.55	-0.45	-0.30	—	-0.35	—	—	-0.30	—
08 738 244	-0.27 <sup>+0.12</sup> <sub>-0.12</sub>	-0.25	—	+0.20*	+0.25	-0.40	-0.35*	—	-0.50	-0.60	-0.20	—	—	-0.55	—	—	-0.35	—
08 750 029	-0.56 <sup>+0.10</sup> <sub>-0.10</sub>	-0.20	—	-0.35*	+0.00	-0.60*	-0.60*	-0.05	-0.60	-0.90*	-0.50*	-0.70	—	+0.35	—	—	-0.65*	—
09 413 057	-0.56 <sup>+0.15</sup> <sub>-0.12</sub>	-0.45	—	-0.05*	+0.10	-0.70	-0.60*	—	-0.85	-0.75	-0.65	—	—	-0.30	—	—	-0.60	—
09 764 965	-0.27 <sup>+0.08</sup> <sub>-0.08</sub>	-0.05	—	-0.10*	+0.00	-0.15*	-0.30*	+0.05	-0.25	-0.45*	-0.30*	-0.30	—	-0.15	—	—	-0.30*	—
09 812 351	-0.90(Fe)	+0.00	—	-0.50*	-0.40	-0.85	-0.90*	—	-0.85	-1.00	-0.85	—	—	-1.20	—	—	-0.65	—
10 119 517	-0.24 <sup>+0.07</sup> <sub>-0.07</sub>	+0.05	—	-0.20*	-0.15	-0.05*	-0.20*	+0.10	-0.35	-0.40*	-0.20*	-0.15	-0.40	+0.40	—	—	-0.25*	—
10 451 090	+0.04 <sup>+0.06</sup> <sub>-0.06</sub>	-0.10	—	+0.10*	+0.00	-0.25	+0.00*	+0.25	-0.15	-0.15	+0.15	+0.00	—	+0.75	—	—	+0.20	—
10 616 594	+0.16 <sup>+0.13</sup> <sub>-0.20</sub>	-0.30	—	+0.00*	-0.35*	+0.05*	+0.05*	+0.10	+0.10*	+0.10*	+0.10*	+0.20*	+0.20*	+0.45	+0.30*	+0.05*	+0.00*	-0.20
10 977 859	-0.11 <sup>+0.07</sup> <sub>-0.06</sub>	-0.05	—	+0.20*	+0.10	-0.05	-0.10*	—	-0.15	-0.35	-0.10	—	—	-0.25	—	—	-0.05	—
11 498 538	-0.15 <sup>+0.07</sup> <sub>-0.07</sub>	-0.15	—	+0.20*	-0.15	-0.15*	-0.20*	-0.15	-0.20	-0.30*	-0.10*	-0.15	-0.40	+0.65	—	—	-0.20*	—
12 353 648	-1.05(Fe)	-0.25	—	-0.55*	-0.25	-0.90*	-1.05*	—	-1.35	-2.05*	-1.25*	—	—	-0.75	—	—	-1.05*	—

the synthetic spectra are calculated using a large library of pre-computed model atmospheres (Table 5) and the analysis runs very fast on up to 300 processor cores of a cluster PC.

Our code GSSP (Grid Search in Stellar Parameters) finds the optimum values of effective temperature  $T_{\text{eff}}$ , surface gravity  $\log g$ , microturbulent velocity  $\xi$ , metallicity  $[M/H]$ , and projected rotational velocity  $v \sin i$  from the minimum in  $\chi^2$  obtained from a comparison of the observed spectrum with the synthetic ones computed from all possible combinations of the before mentioned parameters. The errors of measurement ( $1\sigma$  confidence level) are calculated from the  $\chi^2$  statistics. A detailed description of the method is given in Lehmann et al. (2011) (Paper I).

For the calculation of synthetic spectra, we use the LTE-based code SynthV (Tsymbal 1996) which allows the computation of spectra based on individual elemental abundances. The code uses pre-calculated atmosphere models which have been computed with the most recent, parallelised version

of the LLmodels program (Shulyak et al. 2004). Both programs make use of the VALD database (Kupka et al. 2000) for a pre-selection of atomic spectral lines. The main limitation of the LLmodels code is that the models are well suitable for early and intermediate spectral type stars but not for very hot and cool stars where non-LTE effects or absorption in molecular bands may become relevant, respectively.

The method has been tested on spectra of Vega and successfully applied to *Kepler*  $\beta$  Cep and SPB candidate stars (Paper I). In Paper I, the chemical composition of the stars has been determined by means of an iterative procedure involving (1) the estimation of  $T_{\text{eff}}$ ,  $\log g$ ,  $v \sin i$ ,  $\xi$ , and  $[M/H]$ , (2) the determination of the individual abundances, element-by-element, by fixing all parameters derived in the previous step and taking the abundance table corresponding to the derived metallicity as a first guess, and (3) the re-estimation of  $T_{\text{eff}}$ ,  $\log g$ ,  $v \sin i$ , and  $\xi$  based on the chemical composition evaluated in the second step. In the latest version of

**Table 4.**  $E(B-V)$  determined from the Na D lines,  $T_{\text{eff}}$  obtained from SED-fitting, and the reddening-corrected  $T_{\text{eff}}$ .

KIC	$E(B-V)$	$T_{\text{eff}}$	$T_{\text{eff}}$ (dered)
01 571 152	0.03	6820±140	6980±190
02 166 218	0.01	7050±140	7110±200
03 217 554	0.04	7650±160	7910±250
03 453 494	0.03	7650±150	7840±240
04 847 411	0.05	7290±150	7600±220
05 088 308	0.02	6730±150	6840±190
05 164 767	0.06	6770±130	7100±190
05 446 068	0.04	4950±110	5060±130
05 785 707	0.03	7840±160	8060±260
06 289 468	0.03	8130±170	8300±280
06 509 175	0.08	7080±140	7560±220
06 587 551	0.05	8280±170	8760±350
06 756 386	0.01	7860±150	7930±240
07 748 238	0.05	7150±150	7450±220
08 623 953	0.04	7720±150	7990±250
08 738 244	0.01	8110±160	8190±240
08 750 029	0.05	7250±140	7560±220
09 413 057	0.05	8270±170	8720±340
09 764 965	0.01	7450±170	7510±230
09 812 351	0.01	7750±150	7830±230
10 119 517	0.00	6380±160	6380±160
10 451 090	0.01	7700±160	7750±240
10 616 594	0.00	5240±140	5240±140
10 977 859	0.01	8130±170	8200±260
11 498 538	0.03	6490±160	6530±190
12 353 648	0.02	7350±180	7470±230

**Table 5.** Stellar atmosphere models computed with the LLmodels code for  $\xi = 2 \text{ km s}^{-1}$ .

Parameter, step width					
$[M/H]$	$\Delta[M/H]$	$T_{\text{eff}}$ (K)	$\Delta T_{\text{eff}}$ (K)	$\log g$	$\Delta \log g$
-0.8 - +0.8	0.1	4 500 - 10 000	100	2.5 - 5.0	0.1
		10 000 - 22 000	250	3.0 - 5.0	
Total number of models:					<b>41 888</b>

### 3.2 Results

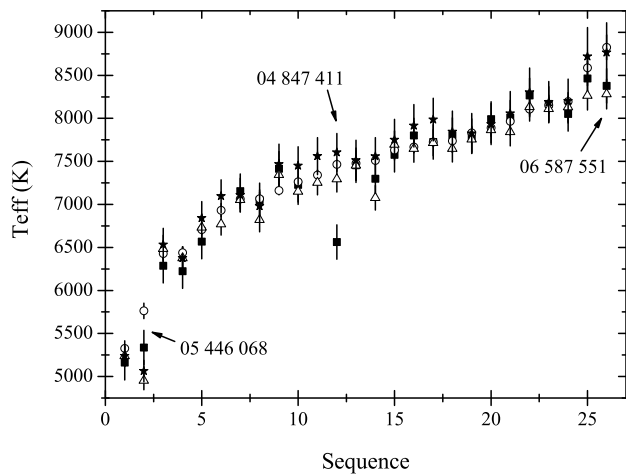
Table 2 summarises the results of spectrum analysis for all 26 stars of our sample. The first four columns of the table represent correspondingly the KIC-number of a star, the effective temperature  $T_{\text{eff}}^{\text{K}}$ , surface gravity  $\log g^{\text{K}}$ , and metallicity  $[M/H]^{\text{K}}$  as is indicated in the KIC. The five following columns list the stellar parameters derived from our spectra, while the last two columns represent the spectral types as estimated from  $T_{\text{eff}}$  and  $\log g$  given in the KIC and determined in this work, respectively. In both cases, the spectral types and the luminosity classes have been derived using an interpolation in the tables by Schmidt-Kaler (1982). We achieve a mean accuracy of about 1% for  $T_{\text{eff}}$ , about  $\pm 0.16$  dex for  $\log g$ , and about 5% for  $v \sin i$ .

Table 3 lists the elemental abundances derived for each target star. The metallicity given in the second column of the table refers to the initially derived chemical composition and was used as initial guess for the determination of the individual abundances. All abundances are given relative to solar values, i.e. negative/positive values refer to an under-/overabundance of the corresponding element compared to the solar composition. We assume the chemical composition of the Sun given by Grevesse et al. (2007) and these values are listed in the header of Table 3 below the element designations. For some of the stars we have reached the metallicity limit in our grid of atmosphere models (KIC 03 217 554, 03 453 494, 09 812 351, and 12 353 648). In these cases, we give the derived Fe-abundance instead of the metallicity. In all other cases, the derived Fe abundance matches the derived metallicity within the measurement error. The abundance errors are estimated to be about  $\pm 0.1$  dex for the elements showing a sufficient number of strong spectral lines in the considered region and about  $\pm 0.2$  dex for the elements represented in the spectrum by only few and rather faint spectral lines.

### 3.3 Special characteristics of some target stars

The derived  $T_{\text{eff}}$  and  $\log g$  are discussed in Sect. 5. Here, we focus on metallicity and abundance anomalies based on Table 3, and on possible binarity of the target stars.

*Stars of lower metallicity.* Only three stars in our sample of 26 show metallicities slightly higher than the Sun; all other stars have lower metallicity. Fifteen stars have a metallicity of more than 0.3 dex lower than the Sun. The four stars of lowest metallicity (KIC 03217554, 03453494, 09812351, and 12353648) show underabundances of the Fe-peak elements and Ca of about 1 dex but much less for Mg and Si. Two of them (KIC 09 812 351 and 12 353 648) have


**Figure 1.** Comparison of  $T_{\text{eff}}$  derived spectroscopically (open circles) with the KIC (filled boxes) and photometric values (open triangles and stars). See text for detailed description.

the GSSP code, we still iterate the individual abundances element-by-element after the first step, but together with  $T_{\text{eff}}$ ,  $\log g$ ,  $v \sin i$ , and  $\xi$ . This allows us to avoid the additional third step. In order to allow the possibility of an incorrect normalisation to be taken into account, and to minimize its influence on the results, we also introduced an additional free parameter that allows the adjustment of the observed continuum relative to the synthetic one during the fitting procedure.

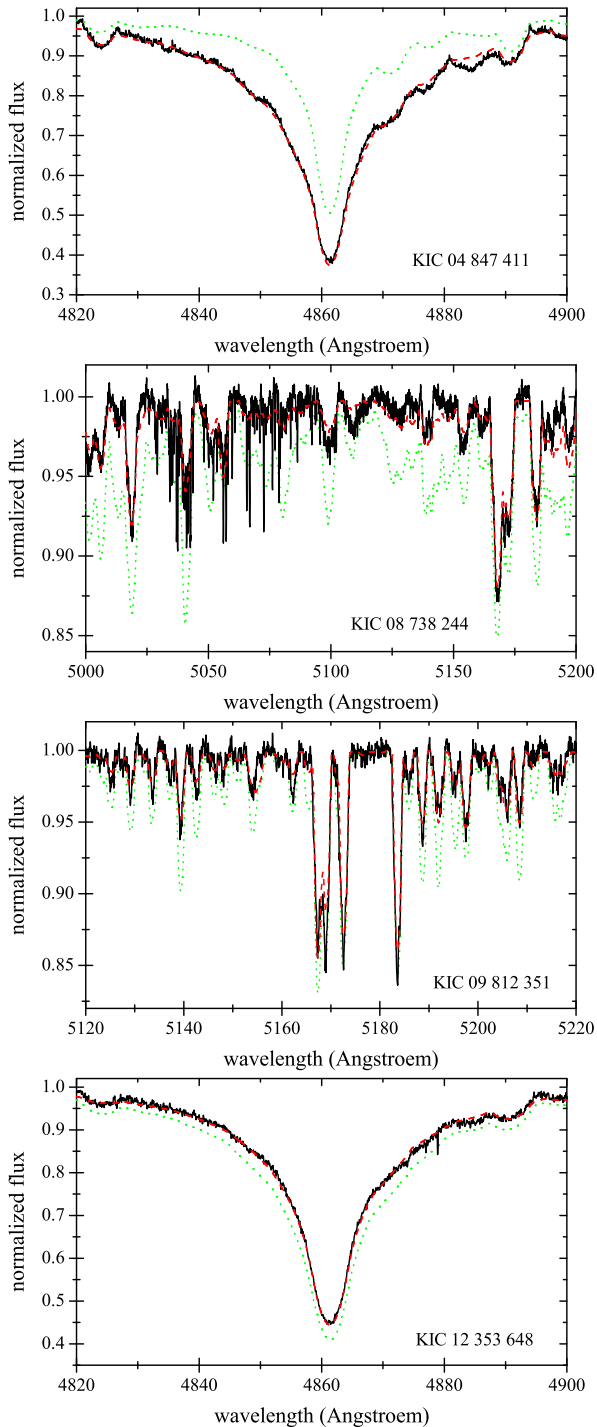


**Figure 2.** Fit of observed spectra (solid, black line) by synthetic spectra calculated from our optimised parameters (dashed, red line) and from the values given in the KIC (dotted, green line), showing either the  $H_{\beta}$  or a metal lines region. A colour plot is provided in the online version.

C abundances comparable to the solar value, resembling the characteristics of  $\lambda$  Boo stars.

*Abundance anomalies.* For eleven of the analysed stars the Ba abundance is found to deviate by more than 0.4 dex from the derived metallicity. In only one of them Ba is underabundant, all other are Ba enhanced. Since the Ba abun-

**Table 6.** The stars for which remarkable differences in the individual RVs are observed.

KIC	BJD-245000	RV ( $\text{km s}^{-1}$ )	dRV ( $\text{km s}^{-1}$ )	max. diff ( $\text{km s}^{-1}$ )
04 847 411	362.552194	2.189	0.058	
	365.476249	2.136	0.137	
	381.512639	-0.968	0.204	
	388.449139	-3.357	0.267	5.5
05 164 767	316.464427	1.493	0.129	
	316.486187	0.798	0.152	
	316.509927	-1.886	0.083	
	318.457963	-0.599	0.109	
	318.479550	0.194	0.123	3.4
06 289 468	338.560657	-0.248	0.285	
	345.482244	-2.466	0.512	
	345.510347	-0.107	0.368	
	345.532246	0.507	0.420	
	345.554214	2.314	0.394	4.8
09 413 057	340.573022	-5.208	0.104	
	351.507244	-6.058	0.082	
	363.430141	0.895	0.540	
	365.404034	7.092	0.736	
10 119 517	376.484499	3.279	0.517	13
	428.472508	-110.03	0.066	
	429.421495	80.42	0.058	
	430.379879	29.61	0.059	190

dance was determined from only one resonance line at  $\lambda$  4934 Å which is known to be strong and sensitive to non-LTE effects, this result must be interpreted with caution.

Most of the stars show overabundances of Mg and Si compared to the derived metallicity, and for eight stars Na is found to be significantly enhanced. Additionally, Ti is found to be depleted in the atmospheres of KIC 05 164 767, 08 750 029 and 12 353 648. For KIC 03 217 554, we did not find consistent results for the iron peak elements, there is a large scatter among the abundances of Fe, Cr, and Ni.

*RV variations.* Five stars in our sample show differences in the measured RVs that are much larger than the errors of measurement. They are listed in Table 6 (note that the RVs are on a relative scale so that the mean RV is zero for each star). From an inspection of the RVs, we suspect for two of these stars (KIC 04 847 411 and 09 413 057) a periodic variation - although the time basis is too short to distinguish between possible periods. KIC 09 413 057 is found by Uytterhoeven et al. (2011b) to be a hybrid pulsator. One of the possible periods that fits the observed RV variations of this star is about 1.6 d and could be caused by pulsations. For one of the five stars (KIC 10 119 517) we observed an extremely large difference in RV of  $190 \text{ km s}^{-1}$  within one day.

#### 4 SPECTRAL ENERGY DISTRIBUTIONS

The effective temperature can also be determined from the spectral energy distribution (SED). For our target stars we constructed SEDs using literature photometry from 2MASS (Skrutskie et al. 2006), Tycho (Hoeg et al. 1997), TASS (Droege et al. 2006), USNO-B1 (Monet et al. 2003) and UCAC3 (Zacharias et al. 2010).  $T_{\text{eff}}$  was determined by

fitting solar-composition Kurucz (1993) model fluxes to the photometry. The model fluxes were convolved with the photometric filter response functions. A weighted Levenberg-Marquardt non-linear least-squares fitting procedure was used to find the solution that minimised the difference between the observed and model fluxes. Since  $\log g$  is poorly constrained due to lack of UV flux measurements, we fixed  $\log g = 4.0$  for all the fits. This introduces additional errors of about 50 K into the determined effective temperature for the stars showing significant deviations from the assumed value of  $\log g$ .

Since spectral energy distributions can be significantly affected by interstellar reddening, we measured the equivalent widths of the interstellar NaD lines if present in our spectra and determined  $E(B-V)$  using the relation given by Munari & Zwitter (1997). Table 4 lists the results. Columns 3 and 4 correspondingly give the temperature values derived without and with the effects of interstellar reddening taken into account.

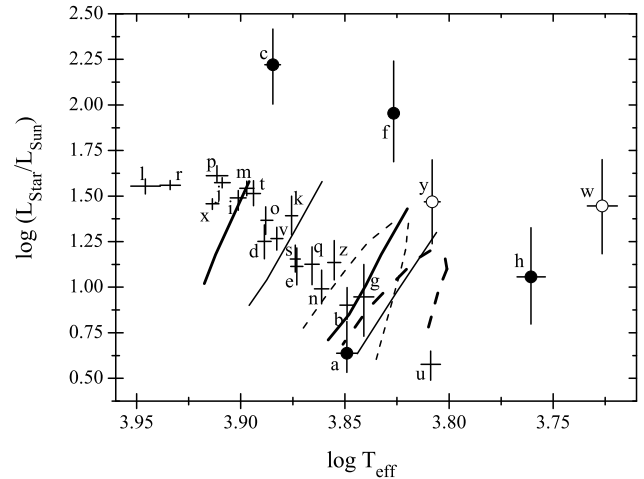
## 5 COMPARISON WITH THE KEPLER INPUT CATALOGUE

Figure 1 compares the spectroscopically derived  $T_{\text{eff}}$  with the photometric and KIC values (typical errors of the KIC data are  $\pm 200$  K for  $T_{\text{eff}}$  and  $\pm 0.5$  dex for both  $\log g$  and metallicity). The stars are sorted by the spectroscopic  $T_{\text{eff}}$  value starting with the coolest object. For most of the targets we find a rather good agreement between the spectroscopically determined temperature (open circles) and the value listed in the KIC (filled boxes). Whereas in most cases the  $T_{\text{eff}}$  from the uncorrected SED fit (open triangles) is slightly lower than the spectroscopic one, the temperatures corrected for the interstellar reddening (asterisks) show rather a good agreement. In the following, we discuss stars that show larger deviations from this general tendency in  $T_{\text{eff}}$  based on Fig. 1 or large deviations from the KIC values in the other parameters based on Table 2.

*KIC 05 446 068*: The spectroscopically derived temperature exceeds the KIC value by 400 K and the de-reddened photometric one by 700 K. Our fit with the best synthetic spectrum is rather poor and the spectrum of a second star can clearly be seen in the residuals. We assume the star to be a SB2 star so that none of the derived temperatures may be valid.

*KIC 06 587 551*: According to the spectroscopic findings, this is the hottest star of our sample, in agreement with the photometrically evaluated  $T_{\text{eff}}$  corrected for the interstellar reddening. Both the KIC and the uncorrected photometric values are by about 500 K lower. This is an interesting fact since we already showed in Paper I that, for the hotter stars ( $T_{\text{eff}} > 8000$  K), the KIC values of  $T_{\text{eff}}$  are systematically lower than the spectroscopic ones, suspecting that the reason may be that the interstellar reddening was not properly taken into account when deriving the KIC temperatures.

*KIC 04 847 411*: This example shows that the parameters listed in the KIC can be unreliable. Figure 2 (top panel) compares the observed  $H_{\beta}$  line profile (solid, black line) with the synthetic ones computed from the parameters derived by us (dashed, red line) and from those listed in the KIC



**Figure 3.** Location of the stars (see Table 7 for labels) and the  $\gamma$  Dor (dashed lines) and  $\delta$  Sct (solid lines) theoretical instability strips in the HR-diagram. Filled circles indicate suspected binaries, open circles the stars for which no reliable fit has been obtained.

**Table 7.** Classification according to the type of variability derived from spectrum and light curve analysis.

KIC	spectroscopic	light curve	label
01 571 152 <sup>1)</sup>			a
02 166 218	$\gamma$ Dors or hybrids	$\gamma$ Dors	b
05 164 767			g
03 453 494			d
06 509 175		hybrids	k
07 748 238			n
09 764 965			s
04 847 411 <sup>3)</sup>	$\delta$ Scts		e
08 623 953			o
08 750 029		$\delta$ Scts	q
09 812 351			t
10 451 090			v
12 353 648			z
06 289 468			j
06 587 551			l
06 756 386		hybrids	m
08 738 244	possibly $\delta$ Scts		p
09 413 057			r
05 785 707		$\delta$ Scts	i
10 977 859			x
05 446 068 <sup>1,2)</sup>		hybrid	h
10 616 594 <sup>2,3)</sup>	too cool	$\delta$ Sct	w
10 119 517		not pulsating	u
03 217 554 <sup>1)</sup>		$\delta$ Sct	c
05 088 308 <sup>1)</sup>	too evolved	$\gamma$ Dor	f
11 498 538 <sup>2)</sup>		no classification	y

<sup>1)</sup> suspected SB2 star; <sup>2)</sup> no reliable fit obtained;

<sup>3)</sup> not analyzed by Uytterhoeven et al. (2011b)

(dotted, green line). Obviously, the green spectrum does not match the observations at all. Since the metallicity value of  $-1.95$  listed in the KIC is much lower than the limiting value in our grid of atmosphere models, we expect the deviation from the observations to be even larger, in particular for all metal lines. Our spectra show RV variations with an amplitude of about  $5.5 \text{ km s}^{-1}$  and a period of  $\sim 10$  d. We need more spectra to reveal the nature of this variability.

*KIC 08 738 244*: This star shows a large discrepancy between the derived values of  $\log g$  and  $[M/H]$  and those listed in the KIC. Figure 2 (second panel) compares the observed spectrum with synthetic spectra in one metal line region and shows that the model based on the KIC values gives no reliable fit. The same is the case for the Balmer line profiles.

*KIC 09 812 351 and 12 353 648*: these are metal poor stars with metallicities below the limit of our grid of atmosphere models. Both show overabundances of C, Mg, and Si compared to the derived Fe abundance, while the spectrum of KIC 12 353 648 additionally exhibits a strong depletion of Ti. The derived metallicities, represented in this case by the Fe abundance, are much lower than the values listed in the KIC and KIC 12 353 648 additionally shows a discrepancy of about 300 K in  $T_{\text{eff}}$ . The effect of the different parameter sets on the synthetic spectra is illustrated in two lower panels of Figure 2.

Figure 3 shows the positions of all stars of our sample in the  $\log(L/L_{\odot})$ - $\log T_{\text{eff}}$  diagram, together with the  $\delta$  Sct and  $\gamma$  Dor instability strips. The latter were reconstructed from Dupret et al. (2005, Figures 2 and 9). The edges of the  $\delta$  Sct instability region have been computed with a mixing-length parameter of  $\alpha=1.8$  for the fundamental mode (solid thin lines) and for a radial order of  $n=4$  (solid thick lines). The edges of the  $\gamma$  Dor instability regions computed with  $\alpha=2.0$  and  $1.5$  are represented by dashed thin and thick lines, respectively. To place the stars into the diagram, we estimated their luminosities from the spectroscopically derived  $T_{\text{eff}}$  and  $\log g$  by means of an interpolation in the tables by Schmidt-Kaler (1982). The luminosity error bars represent a combination of the errors in  $T_{\text{eff}}$  and  $\log g$ , and so in some cases they appear to be significantly larger than the uncertainties in  $T_{\text{eff}}$ . Beside that, the luminosity errors can still be underestimated due to the uncertainties in the empirical relations. Realizing that, we base our classification mainly on the position of the stars in the HR-diagram according to the derived temperatures.

## 6 THE STARS IN THE HR-DIAGRAM

Table 7 classifies the stars according to their type of variability, listing the classifications expected from their location in the HR-diagram (Fig. 3) and derived by Uytterhoeven et al. (2011b) from the frequency analysis of the *Kepler* light curves. There are six “outliers” in the  $\log(L/L_{\odot})$ - $\log T_{\text{eff}}$  diagram (Fig. 3). Three of them (labels c, f, and h) are suspected binaries and two (labels w and y) are the stars for which no reliable fit of the observed spectrum could be obtained. For these objects we cannot give a certain classification. For the remaining, sixth object, KIC 10 119 517 (label u), no pulsations could be found from the light curve analysis.

For most stars of our sample, the classification based

on the light curve analysis appears to be fully consistent with the position of the objects in the  $\log T_{\text{eff}}$ - $\log(L/L_{\odot})$  diagram. We confirm three  $\gamma$  Dor stars (labels a, b, and g), and 10  $\delta$  Sct pulsators lying in the expected region of the HR-diagram. Four of them, however, have been classified by Uytterhoeven et al. (2011b) as hybrid pulsators although they do not fall in the overlapping region between the  $\gamma$  Dor and  $\delta$  Sct stars in our HR-diagram. One star, KIC 04 847 411, was not analyzed by Uytterhoeven et al. (2011b). Its light curve classification listed in Table 7 is based on our own analysis of the first Quarter of *Kepler* data.

There are ten further stars that show  $\delta$  Sct-like oscillations in their light curves. Six of them have been classified by Uytterhoeven et al. (2011b) as hybrid pulsators but do not fall in the overlapping region in the HR-diagram. Five stars (labels i, j, m, p, and x) are close to the hot border of the  $\delta$  Sct instability region, two other ones (labels l and r) are distinctly hotter than given by this border. Four stars are too cool (labels h, w) or too evolved (labels c, f) to be hybrid,  $\gamma$  Dor or  $\delta$  Sct pulsators.

Four stars of our sample are reported by Uytterhoeven et al. (2011b) to be binaries. Three of them could be identified as SB2 stars. For the fourth one, more observations are needed to confirm its binarity spectroscopically.

Fifteen of the analysed targets show metallicities which are lower by more than 0.3 dex than the metallicity of the Sun. The four stars of lowest metallicity show underabundances of about 1 dex. Two of them, KIC 09 812 351 and 12 353 648, have a C abundance comparable to the solar value which might be a sign of  $\lambda$  Boo nature. Additionally to the C abundance, this type of variable stars is characterised by solar abundances of N, O and S. We did not find any spectral lines of these elements in the considered wavelength range that could be used for an abundance determination, however. We also find that most of the analysed stars are rather fast rotators with projected rotational velocities above  $90 \text{ km s}^{-1}$ .

## 7 CONCLUSIONS

We determined the fundamental parameters of 26 stars in the *Kepler* satellite field of view proposed to be candidates for  $\gamma$  Dor-type variables (Uytterhoeven et al. 2011a). The analysis was done by means of the spectrum synthesis method based on the comparison between the observed and synthetic spectra. As an additional test of the derived  $T_{\text{eff}}$ , we computed SEDs by using photometry from literature and determined  $T_{\text{eff}}$  by fitting solar-composition Kurucz (1993) model fluxes to the photometric data.

A comparison of the results from the different methods was made. Besides some outliers, where the reasons can be explained, the  $T_{\text{eff}}$  derived from the spectrum analysis shows a good overall agreement with the values given in the KIC. For the hottest star of our sample, the KIC value appears to be underestimated. This agrees with our finding in Paper I that the  $T_{\text{eff}}$  given in the KIC are in general too low for the hotter stars because the interstellar reddening was not properly taken into account. The  $T_{\text{eff}}$  following from the SED fitting are systematically lower. This can be explained by the interstellar reddening. Our correction for this effect



by using the equivalent widths of the interstellar NaD lines to derive  $E(B-V)$ , improves the situation although in some cases the resulting  $T_{\text{eff}}$  is found to be slightly overestimated. The accuracy of the values for  $\log g$  and  $[M/H]$  in the KIC is rather poor. An uncertainty of  $\pm 0.5$  dex is stated in the catalogue for both parameters, in some cases we also find larger deviations from our analysis so that the values given in the catalogue are not suited to check for the quality of our findings.

The spectroscopically derived fundamental parameters allow us to place the stars in a HR-diagram and to compare their location with the classification made by Uytterhoeven et al. (2011b) based on the oscillation frequencies found in the *Kepler* light curves. In the result, we observed most of the stars in a relative compact region of the diagram that reaches from the cool edge of the  $\delta$  Sct instability strip to a region left of its hot border. For all of the six outliers that are too cool or too evolved to fall into the  $\delta$  Sct instability region we could find an explanation either by binary nature or insufficient convergence of the parameter determination.

We find three stars (labels a, b, and g) out of the 14 stars that show oscillations in their light curves typical for  $\gamma$  Dor or  $\gamma$  Dor- $\delta$  Sct hybrid pulsators that certainly fall into the  $\gamma$  Dor range of the diagram. Ten further stars are found to be located in one of the  $\delta$  Sct regions of the HR-diagram, six of them show  $\delta$  Sct and in four  $\delta$  Sct and  $\gamma$  Dor-typical oscillations co-exist. This shows that oscillations with periods in the  $\gamma$  Dor range are much more common among the  $\delta$  Sct stars than described by the theoretical  $\gamma$  Dor instability region. This finding is in agreement with Grigahcène et al. (2010) who investigated a sample of 234 *Kepler* stars and found a significant number of hybrid pulsators, whereas theory predicts the existence of hybrids in only a small overlapping region of the instability strips.

We find seven stars close to the left or left of the blue edge of the  $\delta$  Sct instability strip calculated for fourth radial overtone pulsations. Only two of these stars show  $\delta$  Sct-like oscillations but five of them show oscillations with periods in the  $\delta$  Sct and in the  $\gamma$  Dor range. Similar to our results, Grigahcène et al. (2010) found a significant number of stars showing  $\delta$  Sct or  $\delta$  Sct- $\gamma$  Dor oscillations which are hotter than predicted by the theoretical blue edge of the  $\delta$  Sct instability strip calculated for fourth radial overtone pulsations.

We found four stars with very low metallicities in the -1 dex range. Two of them have about solar C abundance which could be a sign of  $\lambda$  Boo nature. Both stars show  $\delta$  Sct-like but no  $\gamma$  Dor-typical oscillations. Thus we did not find any hint for a relationship between the  $\lambda$  Boo stars and  $\gamma$  Dor-type variability in our sample.

## ACKNOWLEDGEMENTS

The research leading to these results has received funding from the European Research Council under the European Community's Seventh Framework Programme (FP7/2007–2013)/ERC grant agreement n°227224 (PROSPERITY). This research has made use of the SIMBAD database, operated at CDS, Strasbourg, France.

## REFERENCES

- Aerts, C., Christensen-Dalsgaard, J., & Kurtz, D. W. 2010, *Asteroseismology*, Springer, Heidelberg
- Balona L. A., Krisciunas K., & Cousins A. W. J., 1994, *MNRAS*, 270, 905
- Balona, L. A., Guzik, J. A., Uytterhoeven, K., et al. 2011a, *MNRAS*, 415, 3531
- Balona, L. A., Pigulski, A., Cat, P. D., et al. 2011b, *MNRAS*, 413, 2403
- Borucki W. J., Koch D. G., Basri G., et al., 2011, *ApJ*, 728, 117
- Bruntt H., De Cat P., & Aerts C., 2008, *A&A*, 478, 487
- Cousins, A. W. J. 1992, *The Observatory*, 112, 53
- Cuyppers J., Aerts C., De Cat P., et al., 2009, *A&A*, 499, 967
- De Cat P., Eyer L., Cuyppers J., et al., 2006, *A&A*, 449, 281
- Droege T. F., Richmond M. W., Sallman M. P., & Creager R. P., 2006, *PASP*, 118, 1666
- Dupret M.-A., Grigahcène A., Garrido R., Gabriel M., & Scuflaire R., 2005, *A&A*, 435, 927
- Gilliland R. L., Brown T. M., Christensen-Dalsgaard J., et al., 2010, *PASP*, 122, 131
- Gray, R. O. & Kaye A. B., 1999, *AJ*, 118, 2993
- Grigahcène A., Antoci V., Balona L., et al., 2010, *ApJ*, 713, L192
- Grevesse N., Asplund M., & Sauval A. J., 2007, *Space Sci. Rev.*, 130, 105
- Gustafsson B., Bell R. A., Eriksson K., & Nordlund A., 1975, *A&A*, 42, 407
- Guzik, J. A., Kaye, A. B., Bradley, P. A., Cox, A. N., & Neuforge, C. 2000, *ApJL*, 542, L57
- Handler G., & Shobbrook R. R., 2002, *MNRAS*, 333, 251
- Henry G. W., Fekel F. C., & Henry S. M., 2007, *AJ*, 133, 1421
- Hoeg E., Bässgen G., Bastian U., et al., 1997, *A&A*, 323, L57
- Kaye A. B., Handler G., Krisciunas K., Poretti E., & Zerbi F. M., 1999, *PASP*, 111, 840
- King H., Matthews J. M., Rowe J. F., et al., 2007, *arXiv:0706.1804*
- Krisciunas K., Aspin C., Geballe T. R., et al., 1993, *MNRAS*, 263, 781
- Kupka F. G., Ryabchikova T. A., Piskunov N. E., Stempels H. C., & Weiss, W. W., 2000, *Baltic Astronomy*, 9, 590
- Kurucz R. L., 1979, *ApJS*, 40, 1
- Kurucz R., 1993, *ATLAS9 Stellar Atmosphere Programs and 2 km/s grid*. Kurucz CD-ROM No. 13. Cambridge, Mass.: Smithsonian Astrophysical Observatory, 1993., 13,
- Kurucz R. L., 1995, *Astrophysical Applications of Powerful New Databases*, 78, 205
- Lehmann H., Tkachenko A., Semaan T., et al., 2011, *A&A*, 526, A124
- Marquardt D., 1963, *SIAM J. Appl. Math.*, 11, 431
- Mathias P., Le Contel J.-M., Chapellier E., et al., 2004, *A&A*, 417, 189
- Monet D. G., Levine S. E., Canzian B., et al., 2003, *AJ*, 125, 984
- Munari U., & Zwitter T., 1997, *A&A*, 318, 269
- Paunzen E., Weiss W. W., Heiter U., et al., 1997, *A&AS*, 123, 93
- Paunzen E., 2004, *MNRAS*, 224, 443

- Rodríguez E., & Breger M., 2001, *A&A*, 366, 178
- Rodríguez E., Suárez J. C., Moya A., et al., 2007, *Communications in Asteroseismology*, 150, 131
- Rowe J. F., Matthews J. M., Cameron C., et al., 2006, *Communications in Asteroseismology*, 148, 34
- Sadakane K., 2006, *PASJ*, 58, 1023
- Schmidt-Kaler Th., 1982, in *Landolt-Börnstein*, ed. K. Schaifers, & H. H. Voigt (Springer-Verlag), 2b
- Shulyak D., Tymbal V., Ryabchikova T., Stütz C., & Weiss W. W., 2004, *A&A*, 428, 993
- Skrutskie M. F., Cutri R. M., Stiening R., et al., 2006, *AJ*, 131, 1163
- Tymbal V., 1996, *M.A.S.S., Model Atmospheres and Spectrum Synthesis*, 108, 198
- Uytterhoeven K., et al., 2011a, arXiv:1111.1667
- Uytterhoeven K., Moya A., Grigahcene A., et al., 2011b, *A&A* 543, 125
- Zacharias N., Finch C., Girard T., et al., 2010, *AJ*, 139, 2184